Open Access Research Journal of
Chemistry and Pharmacy
Journals home page: https://oarjpublication/journals/oarjcp/
ISSN: 2783-0276 (Online)

OARJ OPEN ACCESS RESEARCH JOURNALS

(REVIEW ARTICLE)

Check for updates

Sb2Se3 thin films: A brief review of recent developments

HO SOON MIN *

Faculty of Health and Life Sciences, INTI International University, Putra Nilai, 71800, Nilai, Negeri Sembilan, Malaysia.

Open Access Research Journal of Chemistry and Pharmacy, 2023, 03(02), 049–060

Publication history: Received on 07 May 2023; revised on 13 June 2023; accepted on 16 June 2023

Article DOI: https://doi.org/10.53022/oarjcp.2023.3.2.0063

Abstract

This paper presents the preparation synthesis of p-type Sb_2Se_3 films on to various substrates (microscope glass, molybdenum coated glass, fluorine-doped tin oxide glass, and mica) via chemical deposition methods and physical deposition techniques. The properties of the obtained films have been studied by using different tools (x-ray photo electron spectroscopy, x-ray diffraction, atomic force microscopy, high-resolution transmission electron microscopy, Rutherford back scattering, scanning electron microscopy, Raman spectroscopy, energy dispersive x-ray analysis). Thin films showed unique physical, optical, and electoral properties, and have found application in the solar cells (power conversion efficiency in the range of 1.9%-10.57%). X-ray diffraction studies confirmed polycrystalline with orthorhombic phase. Optical studies indicated the band gap in the range of 1.03 eV to 1.85 eV.

Keywords: Antimony triselenide; Thin films; Solar cells; Renewable sources; Band gap; Absorption

1 Introduction

Thin film technology has been applied everywhere in the modern world. Thin film (nanometer to several micrometers) is a layer deposited onto substrate' surface by using different deposition methods [1,2]. The prepared thin films have been used in solar cells [3-5], light-emitting diodes, photodetector [6], biodevices, optoelectronic devices [7], electro luminescence, infrared windows [8,9], flat panel displays, laser devices [10] and sensor devices [11].

Solar energy resources have been used to replace fossil fuels due to renewability. The power conversion efficiency could be improved by controlling the band gap and film thickness [12-14]. Currently, a leading competitor in solar cell technologies is silicon based solar cells. Silicon showed a narrow band gap (about 1.12 eV), and power conversion efficiency was 26.8%. However, this type of solar cell has several disadvantages such as high production cost and relatively high thickness of silicon wafers [15, 16]. Thin film based solar cells have been recognized as second generation photovoltaic technology. They have many advantages including low temperature processes [17], low material cost, low production cost [18], flexibility, and compatibility with mass production [19, 20].

Antimony triselenide (Sb_2Se_3) thin films have orthorhombic phase, showed V-VI type compounds. These materials are low-cost, environment friendly, excellent absorption coefficient (more than $10^5 cm^{-1}$) at room temperature, long carrier lifetime (60 ns) and appropriate band gap value. These binary compounds get rid of complex composition control if compared to CIGS and CZTS films. Also, avoid forming unwanted impurity phases (during the crystallization and deposition process). The Sb_2Se_3 films have been developed in tandem devices due to superior stability and relatively high carrier mobility. Power conversion efficiency of 10.57% was observed when the films were prepared using additive assisted chemical bath deposition method [21]. The Sb_2S_3 (band gap=1.74 eV) and Sb_2Se_3 (band gap=1.22 eV) films were used as top and bottom cell absorber materials in the tandem solar cells, respectively [22]. Experimental results confirmed that this device was able to make up voltage loss in the sub cells, and the power conversion efficiency was 7.93%. To date, researchers have described that single junction solar cells (antimony sulfide or antimony selenide) are dominant and highlighted very limited photo electric conversion efficiency. Therefore, triple-junction antimony based

* Corresponding author: HO SOONMIN

solar cells were developed. An $Sb_2S_3/Sb_2(S_{1-x}Se_x)_3/Sb_2Se_3$ solar cell was designed, and the power conversion efficacy reached 33% [23]. Tarek and co-workers [24] have reported numerical studies of organic/Sb_2Se_3 tandem solar cells. The low band gap (1.23 eV) Sb_2Se_3 and wide band gap organic solar cells (1.72 eV) could be used as bottom (FTO/CdS/Sb_2Se_3/spiro-OMeTAD/Au) and top sub cells (ITO/PEDOT:PSS/DR3TSBDT:$PC_{71}BM$/PFN/Al) in tandem solar cells. The obtained power conversion efficiency of these individual cells was found to be 7.89% and 9.45%, respectively. PEDOT:PSS (conducting polymer) served as hole transport layer, while PFN (semiconducting polymer) as electron transport layer.

Thin film deposition techniques have been categorized into physical methods and chemical deposition techniques. Examples of physical methods such as magnetron sputtering, vacuum evaporation, ion beam evaporation, electron beam evaporation [25], thermal evaporation [26]. Examples of chemical techniques include chemical bath deposition [27,28], successive ionic layer adsorption and reaction [29,30], electro deposition, chemical vapor deposition, sol gel [31, 32], spray pyrolysis and hydrothermal method [33, 34]. Selection of the deposition method is very important during the formation of thin films. There are several criteria (uniformity, film thickness, band gap, composition, and crystallinity) should be focused on in the selection process [35,36].

In the current work, preparation, and properties of Sb_2Se_3 films have been analyzed. Photovoltaic parameters (fill factor, power conversion efficiency, open circuit voltage and short circuit current density) were reported as well.

2 Antimony triselenide films

Antimony is lustrous gray metalloid with chemical symbol “Sb”. The properties of antimony as highlighted in Table 1. Antimony could be employed in flame retardants, lead-acid batteries, and plastics. Antimony compounds have been used as medicines and cosmetics. According to the Table 2, China is the largest producer of antimony (almost 60000 metric tons) in 2022, followed by Russia and Tajikistan [37]. Selenium is a non-metal element with the chemical symbol “Se”. The properties of selenium have been described in Table 1. Selenium could be observed in metal sulfide ores. It produced some allotropes that interconvert with temperature changes. Application of selenium including fertilizers, glass production, alloy, solar cells, photoconductors, and lithium -selenium batteries. According to the Table 3, China is the largest producer of selenium (1120 metric tons) in 2022, followed by Japan and Germany [38].

Table 1 Properties of antimony and selenium

	Antimony	**Selenium**
Atomic number	51	34
Atomic mass	121.76 amu	78.96 amu
Melting point	903.78 K	44 K
Boiling point	1860 K	958 K
Number of protons/electrons	51	34
Number of neutrons	71	45
Density	6.691 g/cm^3	4.28 g/cm^3
Heat of fusion	19.79 kJ/mol	6.69 kJ/mol
Heat of vaporization	193.43 kJ/mol	95.48 kJ/mol
Molar heat capacity	25.23 J/(mol.K)	25.363 J/(mol.K)

Table 2 Worldwide antimony mine production from 2015 to 2022 [37]

	2015 (in metric tons)	**2020 (in metric tons)**	**2021 (in metric tons)**	**2022 (in metric tons)**
China	115000	61000	61000	60000
Russia	9000	25000	20000	20000
Tajikistan	4700	13000	16800	17000
Burma	3500	2200	4600	4000
Australia	5500	3900	4000	4000
Bolivia	5000	2600	2600	2500
Turkey	4500	1330	1300	1300

Table 3 Production volume of selenium globally in 2020 [38]

Country	**Production volume (in metric tons)**
China	1120
Japan	740
Germany	300
Belgium	200
Russia	195
United States	150
Mexico	106
Canada	102
Philippines	100
Finland	84
Poland	74
Peru	53
Sweden	50
Uzbekistan	40
India	10
Serbia	10

3 Literature survey

3.1 Synthesis of thin films using chemical deposition method

Chemical bath deposition method is a very simple deposition method, requiring container and substrate [39]. Several examples of substrates such as fluorine-doped tin oxide (FTO), microscope glass slide, indium tin oxide coated glass slide (ITO), silicon, and soda lime glass have been employed to produce thin films. The chemical bath deposition has been used to produce thin films [40] in highlighted conditions (Sb^{3+} ion = antimony potassium tartrate, Se^{2-} ion = sodium selenosulfite, substrate=glass, duration=10 hours). It is clearly seen that the prepared films were consisted of small particle (4-5 nm) and showed some orientations of nanocrystallines as highlighted in atomic force microscopy (AFM)

and high-resolution transmission electron microscopy (HRTEM) studies, respectively. Rutherford back scattering analysis confirmed stoichiometry of films with some inclusion of oxygen atom.

Uniform, adherent, and reflective films have been deposited on glass slides [41] by using antimony chloride, and sodium selenosulphate (room temperature, 60 minutes). The prepared films indicated polycrystalline phase, several peaks attributed to (220), (330), (430), (060) and (061) planes according to the x-ray diffraction (XRD) patterns. In the x-ray photo electron spectroscopy (XPS) analysis, 54.11 eV and 160.58 eV correspond to Se $3d_{5/2}$ and Se $3P_{3/2}$, respectively. While 766.4 eV and 529.57eV contributed to $Sb3p_{3/2}$ and $Sb3d_{5/2}$, respectively. Optical investigations showed band gap of 1.85 eV, 1.14 eV and 1.3 eV for as-deposited films, annealed sample (100 °C) and annealed sample (200 °C).

A low symmetric crystal structure has been prepared using additive assisted chemical bath deposition method [42] in the presence of sodium selenosulfate and antimony potassium tartrate. Selenourea and thiourea were served as additives to improve the films properties (to reduce Sb-O peak). In the XPS studies, indicated the production of Sb_2Se_3 films and additional peak (Sb-O) in all samples (for Sb 3d region). It is noticeable that different morphologies could be seen in scanning electron microscopy (SEM) images for pure Sb_2Se_3 films (film thickness of 90nm, small grains and several pinholes), Selenourea-Sb_2Se_3 (grain size=435 nm, film thickness of 260 nm) and thiourea-Sb_2Se_3 (film thickness of 170 nm, uniformly covered on the substrate, grain size=290 nm). In terms of the photovoltaic properties, Selenourea-Sb_2Se_3 films showed the highest power conversion efficiency (10.57%), fill factor (67.64%), open circuit voltage (0.467 V), and short circuit current density (33.52 mA/cm^2) if compared to thiourea-Sb_2Se_3 films (open circuit voltage=0.454V, power conversion efficiency=9.17%, fill factor=64.73% and short circuit current density=31.23 mA/cm^2).

The polyol process was a unique soft chemical deposition method for the synthesis of inorganic compounds. This method has many advantages such as ease of use [43], low cost and it is suitable for industrial applications. According to the X-ray diffraction (XRD) results, orthorhombic structure with space group (Pbnm (62) could be observed in the obtained samples [44]. Tiny nanorods showed stronger diffractions {(110) and (040)} if compared to thick nanorods. Raman spectroscopy confirmed that no impurity structures were observed. Several peaks could be seen (figure 1) at 83 cm^{-1}, 118 cm^{-1}, 189 cm^{-1}, 252 cm^{-1}, 356 cm^{-1}, 373 cm^{-1}and 450 cm^{-1}. In addition, higher peak intensities were found, showing enhancement of crystallinity in tiny nanorods. XPS analysis highlighted strong intensity Sb peaks ($3d_{3/2}$=537.87 eV, $3d_{5/2}$=528.47eV), indicating charge state of Sb^{3+}. While valence state of Se^{2-} could be described from $3d_{3/2}$ (53.81 eV) and $3d_{5/2}$ (53.01 eV). In the scanning electron microscopy (SEM) analysis, average diameter was about 6-8 nm with smooth surface in tiny nanorods, while average diameter was more than 90 nm with relatively disordered structure in thick nanorods. Experimental findings revealed that more stable cycling performance (lithium-ion batteries) in tiny nanorod anode materials. The obtained materials displayed excellent discharge capacity (702 mAh/g) at 0.1 C, and successfully maintained the capacity (230 mAh/g, after 100 cycles).

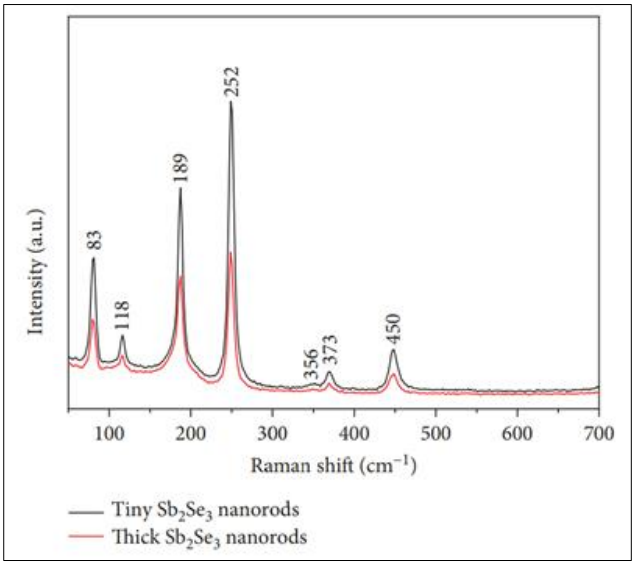

Figure 1 Raman spectrums of the tiny and thick Sb_2Se_3. [44]

High quality films have been synthesized using electro deposition method [45]. During the experiment, silver-silver chloride and platinum sheet were used as reference electrode and counter electrode, respectively. The energy dispersive x-ray analysis (EDX) studies indicated that films prepared (current density of 2-3 A/dm^2) on nickel electrode

(substrate) were close to the stoichiometric composition (atomic percentage of antimony=61.91%, selenium=38.09%). Crystalline, black, and uniform films were deposited on platinum electrode in specific conditions (temperature=338-348K, pH=1.85, annealing temperature=703K). The formation of thin films using chemical deposition method has been reported by many researchers. The physical, optical, and electrical properties of the obtained Sb_2Se_3 thin films have been investigated by using different tools as highlighted in Table 4.

Table 4 Preparation (using chemical deposition methods) and properties of Sb_2Se_3 films

Deposition method	**Highlighted results**
Chemical bath deposition	XRD: orthorhombic phase [46] Band gap: 1.16 eV
Electro deposition	Band gap: 2 eV XRD: Mainly Sb_2Se_3 phase [47] Presence of selenium, antimony and Sb_2Se_3 structure in annealed samples (at 300 °C).
Electro deposition	p-type Sb_2Se_3 films have been deposited on SnO_2 coated glass substrate in acidic conditions [48]. Band gap:1.04 eV Absorption coefficient: more than 10^5 cm^{-1} XRD: orthorhombic phase could be observed in the annealed films (300 °C and argon atmosphere)
Electro deposition	Thin films were deposited onto fluorine doped tin oxide glass substrate (temperature=25 °C, deposition potential=-0.55V). Band gap and crystalline size reduced when the ultrasound waves were employed [49]. Electrical resistance reduced when the temperature was increased.
Electro deposition	Se-rich films indicated rod-like morphology and showed better stability to photo corrosion [50]. The best conditions are described (deposition potential=-0.6V versus Ag/AgCl, precursors=2.5mmol/L SbO and 2 mmol/L H_2SeO_4, total charge density=600 mC/cm^2).
Electro deposition	FESEM: spherical particles XRD: polycrystalline with orthorhombic phase [51]
SILAR	Thin films were prepared onto glass substrate, at temperature of 300 K. XRD: nanocrystalline nature [52] Resistive value: 10^4 to 10^5 Ωcm.
SILAR	Thin films have been synthesized onto different substrates (glass slide, fluorine doped tin oxide glass substrate) at 27 °C. XRD: orthorhombic phase [53] Low power conversion efficiency due to the presence of recombination centre at the interface.
Spray pyrolysis	XRD: amorphous phase (SeO_2), polycrystalline ($CSe(NH_2)_2$). Band gap [54]: 1.28 eV (SeO_2), 1.26 eV ($CSe(NH_2)_2$). Resistivity value: 10^5 to 10^6 Ωcm (SeO_2), 10^7 Ωcm ($CSe(NH_2)_2$).
Spray pyrolysis	Film thickness: 0.5 μm Seebeck coefficient: 46.2 μV/°C in polycrystalline phase, 18.3 μV/°C in amorphous phase [55].

3.2 Deposition of thin films using physical deposition technique

In the close spaced sublimation method, material was heated and then sublimated into gas phase conditions [56]. Following that, transported to the low temperature substrate (surface area) and finally condensed into a nucleus [57]. Absorber layers (p-type Sb_2Se_3) with 4-5 μm thick were prepared via close spaced sublimation technique [58]. XRD patterns of the prepared films were studied using VESTA tool, showed Pbnm space group (figure 2). Several diffraction peaks (221), (301), (211), (002), (310), (212), (041) and (141)) could be detected and matched with the reference card

(JCPDS 15-0861). Raman spectroscopy analysis confirmed three peaks (155 cm^{-1}, 192 cm^{-1}, and 212 cm^{-1}) in the obtained samples. Resistivity, shunt resistance and series resistance values were $5x10^3$ Ω.cm (dark conditions), 86-139 Ω.cm^2 and 8-49 Ω.cm^2, respectively. Photovoltaic parameters such as fill factor (0.34 - 0.46), power conversion efficiency (1.3% - 4.5%), open circuit voltage (433 mV – 593 mV) and short circuit current density (5.2 mA/cm^2 - 22.4 mA/cm^2) were investigated.

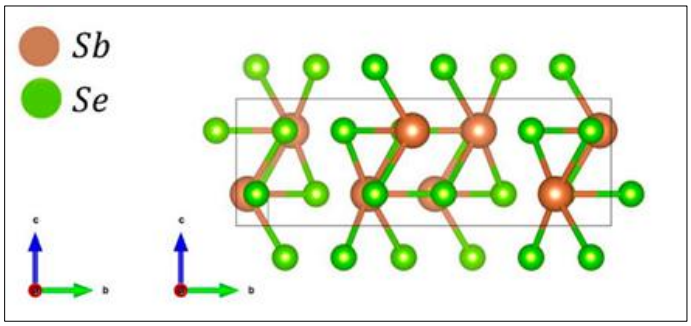

Figure 2 Spatial representation of atoms in the orthorhombic Sb_2Se_3 phase (Pbnm space group) [58]

Preparation of thin films using magnetron sputtering method [59] in the specific conditions (substrates=molybdenum coated glass, sputtering power=35W, sputtering time=90 minutes, working pressure=0.1Pa to 2 Pa). This method offered some advantages including high deposition rate, high purity of films, highly adhesive samples, and uniformity on large area substrates. A stylus profilometer was used to measure film thickness (260 nm to 810 nm). Crack formation occurred when the working pressure is low (0.5 Pa), collision between the sputtered Sb_2Se_3 molecules and argon atoms reduced, resulting in an excessive deposition rate. Also, thin films surface seemed to be irregular and rougher when the working pressure is very low (0.1 Pa). On the other hand, grain size increased with reducing the working pressure (2 Pa to 1 Pa) in the annealed samples, due to facilitate the crystallization of the nanostructured films. Photovoltaic performance was studied in the specific solar cells (glass/Mo/Sb_2Se_3/CdS/ITO/Ag). Fill factor, power conversion efficiency, open circuit voltage and short circuit current density were found to be 53.2%, 5.52%, 448 mV and 24.95 mA/cm^2, respectively. Based on the EQE spectra, higher value could be seen in the highlighted wavelength regions (500 nm to 850 nm), indicating less recombination losses (carriers) in the Sb_2Se_3/CdS heterojunction solar cells. Thin films with micro-size crystal grains were prepared onto molybdenum coated soda lime glass (substrate). Power conversion efficiency was 6.84% (open circuit voltage=504 mV, short circuit current density=24.91 mA/cm^2, fill factor=54.47%) in fabricated solar cell (ITO/CdS/Sb_2Se_3/Mo/glass).

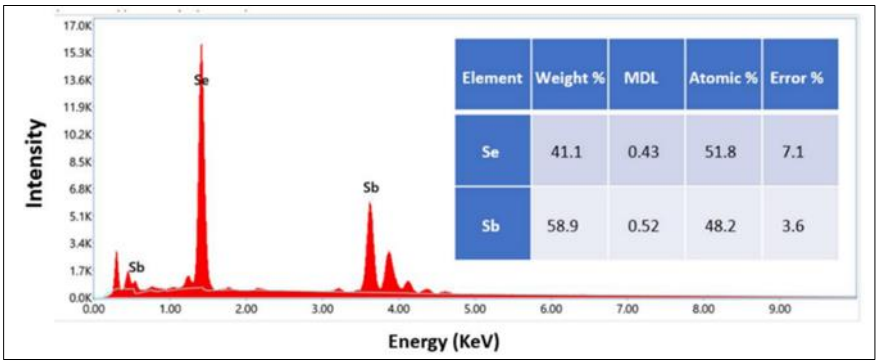

Figure 3 Energy dispersive X-ray analysis for Sb_2Se_3 thin films [60]

Thermal evaporation was used to prepare thin films [60]. Some advantages of this method such as can produce higher purity films, can control the deposition process and little residual gas impurity incorporation. Experimental results confirmed that light absorption (UV-visible regions) could be improved when the films thickness was increased. In the field emission scanning electron microscopy (FESEM) investigations, uniform grains (grain size=15 nm) with pinhole free could be observed. Based on the energy dispersive X-ray analysis (EDX) studies (figure 3), the atomic percentage was 48.2% for antimony and 51.8% for selenium. The band gap reduced when film thickness was increased from 372 nm (1.61 eV) to 640 nm (1.47 eV). Experimental findings indicated that some photons pass through the films if the band gap was too broad. In contrast, more energy will be wasted (as heat) if there is a small band gap. On the other hand, low series resistance (4-20 Ωcm^2) and high shunt resistance (100-500 Ωcm^2) are required to improve high efficiency of the

solar cell devices. Liu and co-workers [61] have prepared thin films onto fluorine-doped tin oxide (FTO) glass. Photovoltaic properties (fill factor=33.5%, power conversion efficiency=2.1%, open circuit voltage=354 mV, short circuit current density=17.84 mA/cm^2) were reported based on solar cell device (FTO/Sb_2Se_3/CdS/ZnO/ZnO:Al/Au). Optical behaviors of polycrystalline (290 °C) and amorphous films (deposited on quartz substrate at room temperature) have been reported by Weiqi and co-workers [62]. In the SEM analysis, film thickness of 635 nm and numerous small clusters could be seen in amorphous phase, while film thickness of 473 nm and larger size (over 2 μm) in polycrystalline phase. A higher band gap could be found in amorphous structure (1.39 eV) if compared to polycrystalline phase (1.03 eV to 1.17 eV). The synthesis of thin films via physical deposition technique has been studied by many scientists. The electrical, physical, and optical properties of the prepared Sb_2Se_3 thin films have been reported using different tools as highlighted in Table 5.

Table 5 Preparation (using physical deposition methods) and properties of Sb_2Se_3 films

Deposition method	**Highlighted results**
Magnetron sputtering	Annealed films (350 °C) indicated power conversion efficiency of 2.1% in specific solar cells (Mo/Sb_2Se_3/CdS/ITO/Ag). SEM: small grains [63] with amorphous phase (as-deposited films), crystalline phase with larger grains (annealed films).
Magnetron sputtering	Highly crystalline with bigger grains could be observed [64]. Power conversion efficiency reached 5.08% in specific solar cells (Mo/Sb_2Se_3/CdS/ITO/Ag).
Magnetron sputtering	Nano rod morphology with well-crystallized phase could be seen in the obtained films [65]. Band gap=1.32 eV Absorption coefficient=10^5 cm^{-1} Power conversion efficiency=2.11%
Magnetron sputtering	Photovoltaic properties (fill factor=37.88 %, power conversion efficiency=2.65%, open circuit voltage=0.32 V, short circuit current density=18.82 mA/cm^2) of the films were reported [66].
Thermal evaporation	XRD: preferred (211) and (221) planes could be observed under argon atmosphere [67]. Preferred (020) and (120) planes under H_2S and H_2Se atmospheres.
Thermal evaporation	Photovoltaic parameters (fill factor=48%, power conversion efficiency=1.9%, open circuit voltage=300 mV, short circuit current density=13.2 mA/cm^2) were reported in CdS/Sb_2Se_3 solar cells [68].
Thermal evaporation	Oxygen addition can enhance power conversion efficiency (4.8%) of the CdS/Sb_2Se_3 heterojunction solar cells. Also, improve open circuit voltage and short circuit current density [69].
Thermal evaporation	Thermogravimetric analysis: decomposition occurred in specific temperature (303 K to 673 K). Raman spectra: two peaks (189 and 210 cm^{-1}) contributed to Ag mode [70].
Ultra-high vacuum molecular beam evaporation	XRD: average crystallite size increased when the evaporation temperature was increased. Raman analysis: blue shift happened when the evaporation temperature increased [71].
Low temperature pulsed electron deposition	The best chemical composition [72] with highly crystalline could be prepared at a specific temperature (200 C to 350 C). Similar morphological for the films prepared synthesized onto various substrates (molybdenum, glass, and fluorine doped tin oxide glass).
Incongruent evaporation	The behaviors dimensions of the islands and surface density were strongly depending on evaporation time and evaporation temperature [73].

Injection vapor deposition	Prepared films showed fewer trap states, low non-radiative recombination loss and minimal deep level defect density [74]. Power conversion efficiency was 10.12%.
Close spaced sublimation	Well-oriented and bigger grains could be observed [75]. Photovoltaic properties (power conversion efficiency=4.32%, fill factor=43.38%, open circuit voltage=0.33 V, short circuit current density=30.19 mA/cm^2) of the films in the solar cells (FTO/TiO_2/Sb_2Se_3/P3HT/Au) were highlighted.
Close spaced sublimation	Power conversion efficiency reached 4.86% in solar cells (glass/Mo/Sb_2Se_3/CdS/ITO/Ag). The highest open circuit voltage was 509 mV due to quasi-vertically oriented structure, with reduced deep level defect density in the solar cells [76].
Molecular beam epitaxy	The streaky lines accompanied by some ordered spots as highlighted in reflection high energy electron diffraction patterns [77]. The Fermi level was found at 0.95 eV as indicated in ultraviolet photo electron spectroscopy.
Vapor transport deposition	XPS: several peaks (528.5 eV and 538.5 eV) contributed to Sb-Se bond in $Sb3_d$. some peaks (53.5 eV and 54.5 eV) contributed to Se^{2-} ion in the $Se3_d$. Photodiode detector [78] was designed (ITO/SnO_2/Sb_2Se_3/Au). High responsivity could be seen in 300-1000 nm, and the highest value of 312 mA/W (at 750 nm)
vapor transport deposition	High quality epitaxial films [79] have been synthesized onto mica substrate (growth rate=0.7 μm/min, 380 °C). AFM: anisotropic morphological with 1D surface rod TEM: zone axes was [210] direction.

4 Conclusion

The p-type Sb_2Se_3 films have been deposited onto different substrates through chemical deposition methods and physical deposition techniques. The properties of the prepared films have been investigated using different tools. Band gap values are in the range of 1.03 eV to 1.85 eV. XRD patterns exhibited amorphous and polycrystalline phase. Photovoltaic parameters were studied, and power conversion efficiency in the range of 1.9%-10.57%.

Compliance with ethical standards

Acknowledgments

This research work was supported by INTI International University.

References

[1] Benbouzid Z, Benstaali W, Rahal L. Efficiency Enhancement by BSF Optimization on Cu (In1−x, Gax) Se2 Solar Cells with Tin (IV) Sulfide Buffer Layer. Journal of Electronic Materials. 2023; 52: 4575–4586.

[2] Saravanan N, Anuar K, Tan W, Ho S, Dzulkefly K, Haron M. Preparation and characterization of PbSe thin films by chemical bath deposition. Jurnal Kimia. 2010; 4: 1-6.

[3] Kashuba A, Andriyevsky B, Kushnir O. Concentration dependences of electronic band structure of CdSe1−xSx thin films. Applied Nanoscience. 2023; 13: 4761–4770.

[4] Gwee S, Anuar K, Tan W, Saravanan N, Ho S. Influence of pH values on chemical bath deposited FeS2 thin films. Pacific Journal of Science and Technology. 2009; 10: 801-805.

[5] Nani R, Ho M, Kassim A. Atomic force microscopy studies of zinc sulfide thin films. International Journal of Advanced Engineering Sciences and Technologies. 2011; 7: 169-172.

[6] Ganesh V, Yahia I. Cerium-Doped Bi2S3 Thin Films Fabricated by Nebulizer-Assisted Spray Pyrolysis Method for Photodetector Applications. Journal of Electronic Materials. 2023; https://doi.org/10.1007/s11664-023-10482-y.

[7] Hassanien A, Darwish A, Qashou S. Fabrication and Description of Amorphous Ge33Se47Sn20 Films for Optical Applications. Journal of Electronic Materials. 2023; 52: 4495–4502.

[8] Barimah E, Boontan A, Steenson D. Infrared optical properties modulation of VO2 thin film fabricated by ultrafast pulsed laser deposition for thermochromic smart window applications. Scientific Reports. 2022; https://doi.org/10.1038/s41598-022-15439-5.

[9] Larciprete M, Centini M, Paoloni S (2020) Adaptive tuning of infrared emission using VO2 thin films. Scientific Reports. 2020; doi: 10.1038/s41598-020-68334-2.

[10] Bartlome R, Strahm B, Sinquin Y. Laser applications in thin-film photovoltaics. Applied Physics B. 2010; 100: 427–436.

[11] Sadekar H, Anil V, Sharma R. Fabrication of CdSe Thin Film for Photosensor Applications. International Journal of Innovations in Engineering and Technology. 2015; 5: 35-41.

[12] Khor L, Saravanan N, Tan W, Ho SM, Anuar K. Effects of deposition time on the chemical bath deposited CuS thin films. Journal of Nepal Chemical Society. 2010; 25: 2-8.

[13] Deepak S, Sakshi C, Dhaka M, Sharma R. An overview on the role of ZnTe as an efficient interface in CdTe thin film solar cells: a review. Materials Advances. 2022; 3: 8081-8107.

[14] Anuar K, Ho S, Saravanan N. Preparation of lead selenide thin films by chemical bath deposition method in the presence of complexing agent (tartaric acid). Turkish Journal of Science & Technology. 2011; 6: 17-23.

[15] Ullah H, Czapp S, Szultka S, Tariq H. Crystalline Silicon (c-Si)-Based Tunnel Oxide Passivated Contact (TOPCon) Solar Cells: A Review. Energies. 2023; https://doi.org/10.3390/en16020715.

[16] Jesus I, Julie D, Mathieu B, Bart M. Carrier-selective contacts using metal compounds for crystalline silicon solar cells. Progress in Photovoltaics. 2023; https://doi.org/10.1002/pip.3552.

[17] Atan S, Ho S, Anuar K, Tan T. Chemical bath deposition of ZnSe thin films: SEM and XRD characterization. European Journal of Applied Sciences. 2011; 3: 113-116.

[18] Lim K, Tan T, Ho S, Anuar K. Morphological characterization of CuS thin films by atomic force microscopy. Research Journal of Applied Sciences, Engineering and Technology. 2011; 3: 513-518.

[19] Arora S, Chuhadiya S, Suthar D. Annealing treatment-induced structural, optical and electrical behaviour of thermally evaporated CuSe films for solar cells. Journal of Materials Science: Materials in Electronics. 2023; https://doi.org/10.1007/s10854-023-10672-8.

[20] Nguyen L, Lee H, Shaikh S, Khan H. Effects of Growth Temperature on the Morphological, Structural, and Electrical Properties of CIGS Thin Film for Use in Solar Cell Applications. Energies. 2023; https://doi.org/10.3390/en16114467.

[21] Zhao Y, Wang S, Li C, Che B. Regulating deposition kinetics via a novel additive-assisted chemical bath deposition technology enables fabrication of 10.57%-efficiency Sb2Se3 solar cells. Energy & Environmental Science. 2022; 15: 5118–5128.

[22] Zhang J, Lian W, Yin Y, Wang X. All antimony chalcogenide tandem solar cell. Solar RRL. 2020; https://doi.org/10.1002/solr.202000048.

[23] Cao Y, Liu C, Jiang J, Zhu X. Theoretical Insight into High-Efficiency Triple-Junction Tandem Solar Cells via the Band Engineering of Antimony Chalcogenides. Solar RRL. 2021; DOI: 10.1002/solr.202000800.

[24] Tarek I, Agwa M, Alanazi M, Habib K. Proposal and Numerical Analysis of Organic/Sb2Se3 All-Thin-Film Tandem Solar Cell. Polymers. 2023; https://doi.org/10.3390/polym15112578.

[25] Asmar R, Zaouk D, Foucaran A. Characterization of electron beam evaporated ZnO thin films and stacking ZnO fabricated by e-beam evaporation and rf magnetron sputtering for the realization of resonators. Microelectronic Engineering. 2006; 83: 393-398.

[26] Benyahia K, Aida M, Benhaya A. ZnS thin films deposition by thermal evaporation for photovoltaic applications. Journal of Semiconductors. 2015; DOI 10.1088/1674-4926/36/10/103001.

[27] Akmal Z, Azrul G, Ahmad I, Ahmad W. Effect of Chemical Bath Deposition Variables on the Properties of Zinc Sulfide Thin Films: A Review. Molecules. 2023; DOI: 10.3390/molecules28062780.

[28] Ho SM, Vyas C, Patel K. A short review of CdTe and CdSe films: growth and characterization. Mediterranean Journal of Chemistry. 2018; 7: 115-124.

[29] Gerasin V, Pogodin I, Kurenkov V. Successive Modification of Montmorillonite with Quaternary Alkylammonium Salts of Various Structures as a Method of Preparing Nanofillers for in situ Synthesis of Polymer Nanocomposites (SILAR)-Deposited CuO Thin Films of Nitrobenzene. Russian Journal of Applied Chemistry. 2022; https://doi.org/10.1134/S1070427222020112.

[30] Sankapal B, Mane R, Lokhande C. Preparation and characterization of Sb2S3 thin films using a successive ionic layer adsorption and reaction (SILAR) method. Journal of Materials Science Letters. 1999; 18: 1453–1455.

[31] Brien S, Koh L, Copuroglu M. Structural and Physical Characterisation of Zinc Oxide Thin Films Prepared from Zinc Acetate via the Sol-gel Method. MRS Online Proceedings Library. 2007; https://doi.org/10.1557/PROC-1035-L05-09.

[32] Yakuphanoglu F. Preparation of nanostructure Ni doped CdO thin films by sol gel spin coating method. Journal of Sol Gel Science and Technology. 2011; 59: 569–573.

[33] Joissy M, Anila E. Hydrothermal assisted chemical bath deposition of (Cd:Zn)S thin film with high photosensitivity and low dark current. Solar Energy. 2018; 172: 165-170.

[34] Krajian H, Abdallah B, Kakhia M. Hydrothermal growth method for the deposition of ZnO films: Structural, chemical and optical studies. Microelectronics Reliability. 2021; https://doi.org/10.1016/j.microrel.2021.114352.

[35] Bakiyaraj G, Dhanasekaran R. Synthesis and characterization of flower-like ZnSe nanostructured thin films by chemical bath deposition (CBD) method. Applied Nanoscience. 2013; 3: 125–131.

[36] Indirajith R, Ahamed M, Ramamurthi K. Synthesis of ZnSe Nano Particles, Deposition of ZnSe Thin Films by Electron Beam Evaporation and Their Characterization. Ferroelectrics. 2014; 467: 13-21.

[37] https://www.statista.com/statistics/264958/antimony-production/

[38] https://www.statista.com/statistics/1312522/selenium-production-volume-worldwide-by-country/#:~:text=The%20country%20with%20the%20largest,3.33%20thousand%20metric%20tons%20worldwide.

[39] Asmaa N, Moria H, Bais B, Hiba A. Mechanism of Chemical Bath Deposition of CdS Thin Films: Influence of Sulphur Precursor Concentration on Microstructural and Optoelectronic Characterizations. Coatings. 2022; https://doi.org/10.3390/coatings12101400.

[40] Lokhande D, Muller M, Ganesan V, Mane R. XRD, SEM, AFM, HRTEM, EDAX and RBS studies of chemically deposited Sb2S3 and Sb2Se3 thin films. Applied Surface Science. 2002; 193: 1–10.

[41] Anu K, Melda F, Lakshmi M. Effect of selenisation on the properties of antimony selenide thin films. IOP Conference Series Materials Science and Engineering. 2020; doi:10.1088/1757-899X/872/1/012151.

[42] Yuqi Z, Chen H, Chen T, Li C. Regulating deposition kinetics via a noveladditive-assisted chemical bath deposition technology enables fabrication of 10.57%-efficiency Sb2Se3 solar cells. Energy & Environmental Science. 2022; DOI: 10.1039/d2ee02261c.

[43] Fievet F, Viau G, Sixard L, Chau F. The polyol process: a unique method for easy access to metal nanoparticles with tailored sizes, shapes and compositions. Chemical Society Reviews, 2018; 47: 5187-5233.

[44] Yuan T, Chen Z, Zhao Y, Sun Z. One-Dimensional Sb2Se3 Nanorods Synthesized through a Simple Polyol Process for High-Performance Lithium-Ion Batteries. Journal of Nanomaterials. 2018; https://doi.org/10.1155/2018/4273945.

[45] Vusala A, Akif S, Parvin H, Dunya M. Electrodeposition of the Sb2Se3 thin films on various substrates from the tartaric electrolyte. Journal of Electrochemical Science and Engineering. 2019; DOI: https://doi.org/10.5599/jese.676.

[46] Meherzi H, Ben T, Dachraoui M. Synthesis, structure and optical properties of Sb2Se3. Materials Science in Semiconductor Processing. 2013; 16: 179-184.

[47] Fernandez A, Merino M. Preparation and characterization of Sb2Se3 thin films prepared by electrodeposition for photovoltaic applications. Thin Solid Films. 2000; 366: 202-206.

[48] Yanqing L, Li J, Liu Y, Jiang L, Han C. Preparation and characterization of Sb2Se3 thin films by electrodeposition and annealing treatment. Applied Surface Science. 2012; 261: 510-514.

[49] Behrouz B, Farid J, Mohsen C. Electro-sonical deposition of nanostructured Sb2Se3 films for optoelectronic applications. Journal of Alloys and Compounds. 2021; https://doi.org/10.1016/j.jallcom.2020.157308.

[50] Magno B, Lucas S, Lucia H. Electrodeposition Conditions Effect Sb2Se3 Thin-Film Properties. ChemElectroChem. 2019; 6: 2937-2944.

[51] Farid J, Mohsen C, Behrouz B. Optoelectronic properties of nanostructured Sb2Se3 films synthesized by electrodeposition method: Effect of Zn concentrations. Sensors and Actuators A: Physical. 2022; https://doi.org/10.1016/j.sna.2022.113750.

[52] Lokhande D, Ganesan V, Sartale S, Pathan H. A novel method for the deposition of nanocrystalline Bi2Se3, Sb2Se3 and Bi2Se3–Sb2Se3 thin films—SILAR. Applied Surface Science. 2001; 182: 413-417.

[53] Sankapal R, Lokhande D. Studies on photoelectrochemical (PEC) cell formed with SILAR deposited Bi2Se3–Sb2Se3 multilayer thin films. Solar Energy Materials and Solar Cells. 2001; 69: 43-52.

[54] Rajpure Y, Bhosale C. Effect of Se source on properties of spray deposited Sb2Se3 thin films. Materials Chemistry and Physics. 2000; 62: 169-174.

[55] Rajpure Y, Bhosale H, Lokhande D. A comparative study of the properties of spray-deposited Sb2Se3 thin films prepared from aqueous and nonaqueous media. Materials Research Bulletin. 1999; 34: 1079-1087.

[56] Kazi S, Halina M, Amin N. Influence of deposition time in CdTe thin film properties grown by Close-Spaced Sublimation (CSS) for photovoltaic application. Results in Physics. 2019; https://doi.org/10.1016/j.rinp.2019.102371.

[57] Amin N, Karim M, Othman Z. An In-Depth Analysis of CdTe Thin-Film Deposition on Ultra-Thin Glass Substrates via Close-Spaced Sublimation (CSS). Coatings. 2022; https://doi.org/10.3390/ coatings12050589.

[58] Pasini S, Spoltore D, Parisini A, Foti G. Sb2Se3 Polycrystalline Thin Films Grown on Different Window Layers. Coatings. 2023; https:// doi.org/10.3390/coatings13020338.

[59] Rong T, Zhang X, Fan P, Liang G, Luo Y. Controlled Sputtering Pressure on High-Quality Sb2Se3 Thin Film for Substrate Configurated Solar Cells. Nanomaterials. 2020; doi:10.3390/nano10030574.

[60] Kumari R, Yadav C, Kumar R. Thermally Deposited Sb2Se3/CdS-Based Solar Cell: Experimental and Theoretical Analysis. Nanomaterials. 2023; https://doi.org/10.3390/nano13061135.

[61] Liu X, Han H, Tang J, Qin S, Lu L. Thermal Evaporation and Characterization of Sb2Se3 Thin Film for Substrate Sb2Se3/CdS Solar Cells. ACS Applied Materials & Interfaces. 2014; 6: 10687–10695.

[62] Weiqi L, Ying Z, Luo M, Liu X, Zeng K. Optical properties of amorphous and polycrystalline Sb2Se3 thin films prepared by thermal evaporation. Applied Physics Letters. 2015; http://dx.doi.org/10.1063/1.4927741.

[63] Tang R, Chen X, Fan P, Liang G. Magnetron sputtering deposition and selenization of Sb2Se3 thin film for substrate Sb2Se3/CdS solar cells. Surface and Coatings Technology. 2019; 360: 68-72.

[64] Guangxing L, Chen X, Li Y, Liu Y, Tang R. Spark plasma sintering of Sb2Se3 sputtering target towards highly efficient thin film solar cells. Solar Energy Materials and Solar Cells. 2020; https://doi.org/10.1016/j.solmat.2020.110530.

[65] Hu J, Bo F, Fa P, Luo J. Facile preparation and enhanced photoelectrical performance of Sb2Se3 nano-rods by magnetron sputtering deposition. Solar Energy Materials and Solar Cells. 2017; 160: 257-262.

[66] Shuo C, Zheng Z, Su Z, Fan P, Liang G. Magnetron sputtered Sb2Se3-based thin films towards high performance quasi-homojunction thin film solar cells. Solar Energy Materials and Solar Cells. 2019; https://doi.org/10.1016/j.solmat.2019.110154.

[67] Leng Z, Wu K, Yu J, Wei Y. Sb2Se3 films fabricated by thermal evaporation and post annealing. Vacuum. 2021; https://doi.org/10.1016/j.vacuum.2020.109840.

[68] Miao L, Leng M, Liu X, Chen J, Chen C. Thermal evaporation and characterization of superstrate CdS/Sb2Se3 solar cells. Applied Physics Letters. 2014; https://doi.org/10.1063/1.4874878.

[69] Xinsheng L, Chao C, Wang L, Luo M, Xue D. Improving the performance of Sb2Se3 thin film solar cells over 4% by controlled addition of oxygen during film deposition. Progress in Photovoltaics. 2015; 23: 1828-1836.

[70] Raja S, Asokan K, Mohd Z. Mitigation of Surface Oxidation in Sb2Se3 Thin Films Via Te Doping: An Effective Strategy Towards Realization of Efficient Electronic Devices. The Journal of Physical Chemistry C. 2022; 126: 6065–6074.

[71] Fantini C, Gonzalez J, Moreira B. Growth and optical properties of nanocrystalline Sb2Se3 thin-films for the application in solar-cells. Solar Energy. 2020; 211: 613-621.

[72] Pattini F, Sidoli M, Sala A, Gilioli E. Role of the substrates in the ribbon orientation of Sb2Se3 films grown by Low-Temperature Pulsed Electron Deposition. Solar Energy Materials and Solar Cells. 2020; https://doi.org/10.1016/j.solmat.2020.110724.

[73] Oleg R. Growth and morphology of SbSe based island films, Advanced Materials Research. 2014; https://doi.org/10.4028/www.scientific.net/AMR.875-877.1387.

[74] Zhaoteng D, Wang S, Mai Y, Li Z, Ying W. Sb2Se3 Thin-Film Solar Cells Exceeding 10% Power Conversion Efficiency Enabled by Injection Vapor Deposition Technology. Advanced Materials. 2022; https://doi.org/10.1002/adma.202202969.

[75] Laurie J, Peter Y, Oliver S, Tom B. Close spaced sublimation for Sb2Se3 solar cells. IEEE Photovoltaic Specialists Conference, 25-30 June, 2017, Washington DC, United States. DOI: 10.1109/PVSC.2017.8366746.

[76] Zhuang Z, Shuo C, Xiang H, Liang G. Quasi-Vertically Oriented Sb2Se3 Thin-Film Solar Cells with Open-Circuit Voltage Exceeding 500 mV Prepared via Close-Space Sublimation and Selenization. ACS Applied Materials & Interfaces. 2021; 13: 46671–46680.

[77] Chen Y, Chong C, Han H, Chuang P. The heterostructure and electrical properties of Sb2Se3/Bi2Se3 grown by molecular beam epitaxy. Chinese Journal of Physics. 2019; 62: 65-71.

[78] Sen W, Yin X, Xie H, Guo Y. Vapor transport deposition of Sb2Se3 thin films for photodetector application. Journal of Advanced Dielectrics. 2020; DOI: 10.1142/S2010135X20500162.

[79] Lukas V, Kim K, Wang G, Fanny H. Surface and interface structures of epitaxial Sb2Se3 on mica. Applied Surface Science. 2021; https://doi.org/10.1016/j.apsusc.2021.150859.